Available online at www.sciencedirect.com
SCIENCE DIRECT®

Signal Processing: *Image Communication* ▮ (▮▮▮▮) ▮▮▮–▮▮▮

SIGNAL PROCESSING:
IMAGE
COMMUNICATION

www.elsevier.com/locate/image

Downsampling dependent upsampling of images

Tamás Frajka[1], Kenneth Zeger*,[1]

University of California, San Diego, Department of Electrical and Computer Engineering, 9500 Gilman Dr, MC0407, La Jolla, CA 92093-0407, USA

Received 8 April 2003; received in revised form 10 August 2003; accepted 2 October 2003

Abstract

Downsampling an image results in the loss of image information that cannot be recovered with upsampling. We demonstrate that the particular combination of downsampling and upsampling methods used can significantly impact the reconstructed image quality, and then we propose a technique to identify patterns associated with different downsampling methods in order to select the appropriate upsampling mechanism. The technique has low complexity and achieves high accuracy over a wide range of images.

Keywords: Image resizing; Downsampling; Upsampling

1. Introduction

Digital imagery can be viewed on various different display sizes, depending on the electronic device being used (e.g. computer monitor, laptop computer screen, PDA, cell phone, etc.). Similarly, digital cameras offer a wide range of image resolutions, yielding images of various different sizes.

The choice of display size is typically determined by some constraint on the device, such as its size, price, quality, etc. Often small display sizes are used on devices with limited amounts of on-board memory. If a large amount of memory is available, a full resolution image can be stored and locally subsampled for viewing on the given screen size. However, if the on-board memory is tightly limited this may not be a feasible option. In such a case, typically the device could either store the appropriate resolution image or only some portions of the original.

A lower resolution image can be obtained by manipulating the image in the spatial domain. A comparison of some of these techniques for image resampling is given in [12]. When transmitted over limited bandwidth communication channels, images are often compressed to conserve resources.

Image compression algorithms need to allow flexibility in choosing a decompression resolution. This property is called "spatial scalability". With spatial scalability different devices can decode different resolution versions of the same image without having to encode the same image to

*Corresponding author.

E-mail addresses: frajka@code.ucsd.edu (T. Frajka), zeger@ucsd.edu (K. Zeger).

[1] The research was supported in part by the National Science Foundation and the UCSD Center for Wireless Communications.

several different decoding resolutions. Both the original JPEG standard and the more recent standard, JPEG2000, have built-in modes for spatial scalability.

Once a lower resolution image is decoded, a display device typically does not have access to the full resolution image any more. If the user wants to resend the image to a different receiver whose device is capable of displaying the image at a higher resolution, the image needs to be upsampled at the receiver to make full use of the display's capabilities.

A challenging task in image upsampling is to best preserve the sharpness of the edges in the image. Traditional spline-based methods [7,10,13] result in sharper edge reconstruction when compared with linear filtering approaches. Yang and Nguye n [14] proposed interpolated Mth band filters for image size conversion and achieve some improved image quality. Edge-directed methods [1,8] seek to identify edges at a subpixel level in the downsampled image and avoid their smoothing in the resizing operation. Atkins et al. gave two methods [3,4] that aimed to locally find an appropriate filter for the scaling of each pixel. Both methods require training for the classifier and the selection of each filter's parameters, but they differ in the particular classification technique used.

All of the above techniques process an image in the spatial domain. A transform domain approach was taken by Chang et al. [5]. Their solution is based on the evolution of the local minima and maxima in the different frequency bands of the wavelet transformed image. These local extrema corresponding to edges in the spatial domain are used to estimate the high frequency coefficients that are lost in the downsampling process.

Dugad and Ahuja [6] introduced an image resizing method using the discrete cosine transform (DCT) that showed improved image quality when compared with bilinear spatial domain interpolation. They also found that this method performs well on images that were downsampled using bilinear interpolation. Mukherjee and Mitra [11] presented a modification of this technique based on subband DCT [9] and extended Dugad and Ahuja's method to color images.

In this paper, we confirm that the performance of the upsampling process depends on the particular upsampling method as well as the downsampling method used to obtain the lower resolution image. We propose a method that estimates the type of downsampling method used by looking for "signatures" of different techniques in the downsampled image. Using this type-estimate we choose a specific upsampling method that results in improved image quality. In many cases the different upsampling methods result in seemingly similar images, but these images may differ by 1–8.5 dB when compared with the original image. The differences usually occur in the reconstruction of the image edges which can be visually significant if the upsampled image is subject to further image processing or edge detection-based image analysis.

Section 2 demonstrates the importance of using the appropriate upsampling method for a given downsampled image. Section 3 describes our proposed method. Simulation results are shown in Section 4 and we conclude in Section 5.

2. Subsampling dependent upsampling

Subsampling followed by upsampling is an inherently lossy process, so that the resulting image will differ from the original. The information lost in downsampling cannot in general be fully recovered. With a correct choice of an upsampling method, one can avoid introducing further distortion into the reconstruction process.

In order to demonstrate that different combinations of downsampling and upsampling techniques yield different results we used the following experiment. A set of test images was downsampled to one fourth of the images' original sizes (i.e. each dimension was divided in half) and then resampled to the original resolution. The following three methods were used for subsampling:

- *Bilinear*: the subsampled value is the average of the four corresponding intensity values.
- *DCT*: for each 8×8 block in the original image, a DCT is performed. Using only the top left 4×4 block of DCT coefficients in each 8×8

block, a 4 × 4 inverse DCT is performed (see [6] for more details).

- *Wavelet*: a single level wavelet transform is performed using 9-7 filters [2]. The appropriately scaled LL band gives the subsampled image.

Similarly, the upsampling methods in the experiment are the following:

- *Bilinear*: The upsampling inserts zeros between every two samples of the downsampled image and performs a bilinear interpolation.
- *DCT*: The image is processed in 4 × 4 blocks, with the DCT performed on each block. The 4 × 4 DCT blocks are then placed in the upper left corner of an 8 × 8 block of all zeros and the inverse DCT is performed on the 8 × 8 blocks (see [6]).
- *wavelet*: The image to be upsampled is taken (with appropriate scaling) to be the LL band of a single level wavelet transform with all high frequency bands set to zero, and the inverse wavelet transform is performed using 9-7 filters.

The tables in Appendix A indicate that the particular subsampling-upsampling combination can have a significant quantitative effect on the PSNR of the reconstructed image. Depending on the image and the combinations, the difference between the worse and best can be up to 8.5 dB!

It is also clear that bilinear interpolation-based upsampling is never optimal. DCT-based upsampling is preferred for images that result from DCT-based or bilinear subsampling. DCT-based upsampling outperforms bilinear upsampling in the high-frequency areas of the images. Bilinear upsampling is a simple averaging operation, and it cannot recover high-frequency information. DCT-based upsampling however can preserve some high-frequency content due to its implementation, as described above.

Wavelet upsampling performs best for images obtained with wavelet-based downsampling. This particular combination achieved the best overall PSNR for 84% of the test images. Any combination of wavelet-based and bilinear or DCT-based operation yields poor performance due to the filters not being matched to each other.

The PSNR results are important in applications where the image is further subjected to some processing or if it is used for differential coding. For human observers, the visual image quality is important. Fig. 1 shows a comparison between the reconstructed Lena images. The downsampling method is the same (wavelet-based), and the difference is in the upsampling: wavelet-based versus DCT-based. Even though wavelet-based

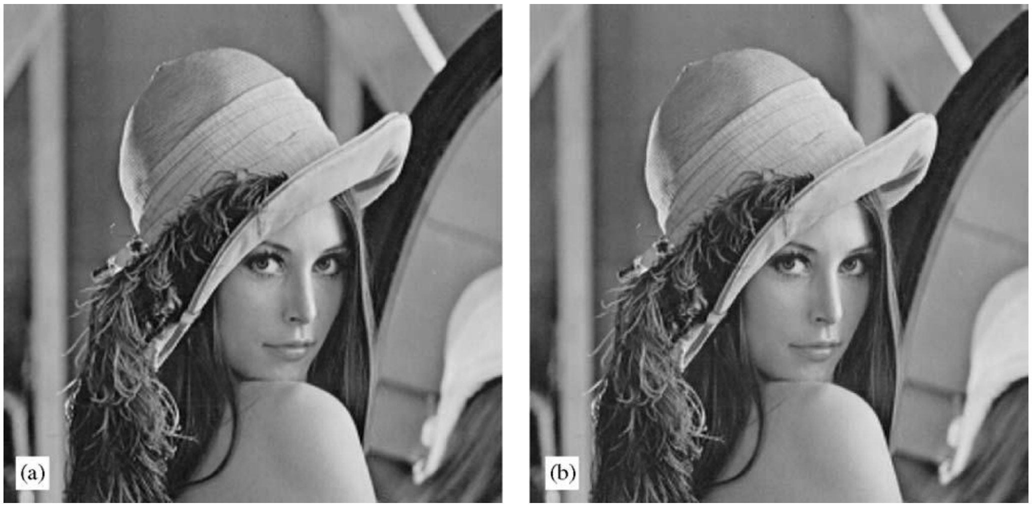

Fig. 1. Reconstructed Lena image with wavelet-based downsampling and (a) wavelet-based upsampling (35.25 dB), (b) DCT-based upsampling (30.19 dB).

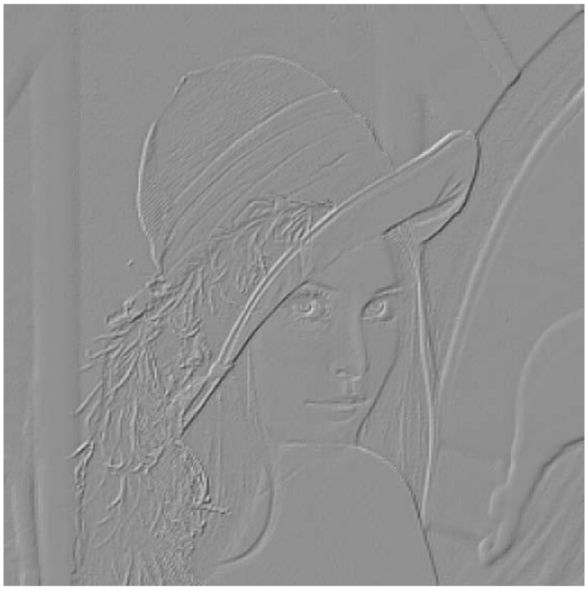

Fig. 2. The rescaled difference of images Fig. 1 (a) and (b). Medium gray levels indicate where the two are identical. The differences are the dark and bright colored areas.

upsampling results in an image that is 5.06 dB better than the DCT-based image, the differences are visually very small.

Fig. 2 shows where the two images differ. It was obtained by rescaling the difference image between images (a) and (b) in Fig. 1. Pixels that are medium gray indicate where the two images are identical; darker and lighter pixels show where they differ. The differences occur around the edges, while the smooth areas are reconstructed the same.

3. Proposed algorithm

The different subsampling techniques yield slightly different images at lower resolution. Most of the differences concentrate around the edge regions of these images. All three techniques discussed here can be thought of as a filtering followed by decimation. Fig. 3 shows the 1-D filter response to the step edge (0 to 1, and 1 to 0 transitions) profiles before decimation for the bilinear, DCT, and wavelet methods. In the bilinear and wavelet cases the filters are given. In the DCT case the filter response was compiled from the subsampled version of two step edges that are shifted one position with respect to each other. (Note that in the DCT case the response also slightly varies depending on the location of the edge within the boundaries of the 8×8 blocks.)

These figures indicate that the edge response of the bilinear and DCT cases are similar in slope, being close to a smooth linear transition. The wavelet response trails below the linear slope in the case of the rising edge, while it goes above the linear slope in the case of the falling edge.

In the downsampled image only half of these edge points are present. Depending on the location of an edge in the image, it is represented by either the odd or the even samples of these transitions. These samples of the profiles are characteristic of the particular downsampling operation. Here we propose an algorithm that tries to locate these step edge responses in a downsampled image as indicators of the subsampling technique used.

In our proposed method we use blocks formed from the odd and even samples of the profiles shown in Fig. 3 as “signatures” of the downsampling technique. As these profiles are characteristic of the downsampling method, the signatures are image independent. They identify the subsampling method in the downsampled image. In the case of a vertical step edge, identical rows of the samples of the profiles form the block, while for horizontal step edges these samples are placed in the columns. Since a feature in an image is considered an edge if its length spans several pixels, the number of these identical columns or rows should be greater than one. However, very few real life images have long vertical or horizontal step edges. Thus in practical cases the blocks should be kept relatively small in order to find reliable matches. We found that a block size of 4×4 presents a good trade-off between these two constraints.

A signature set of a downsampling method contains a total of eight signatures: the odd samples and the even samples of the rising and falling step edge responses for both vertical and horizontal edges.

As noted in Section 2, DCT-based upsampling is preferred for both bilinear and DCT-based downsampling. The step edge response of the two cases

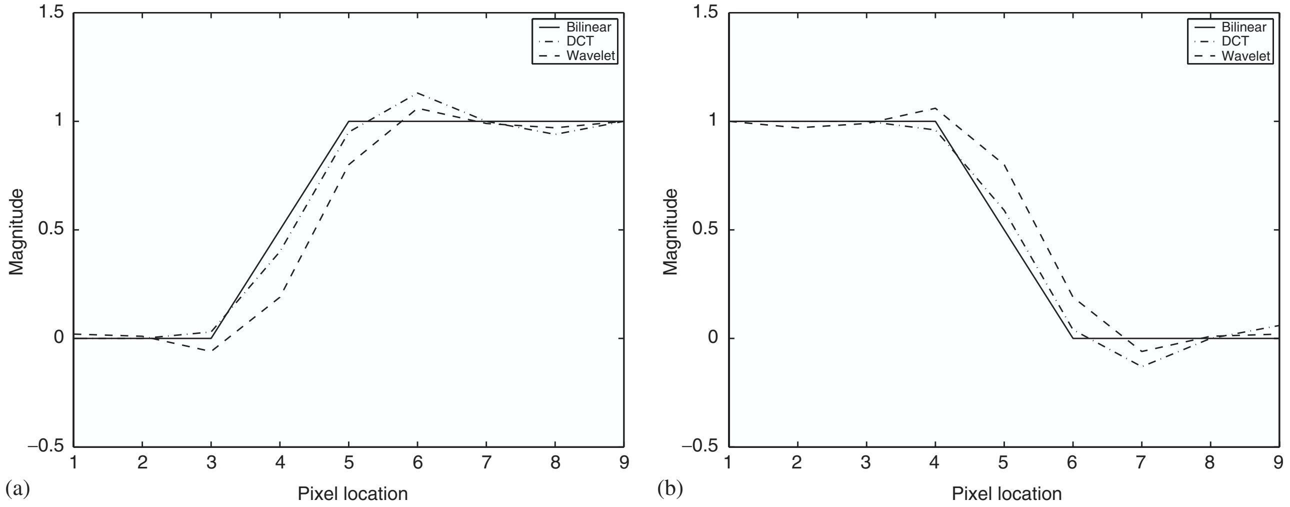

Fig. 3. Edge response of the bilinear, DCT, and wavelet "filtering" for (a) a rising step edge, (b) a falling step edge. These curves indicate the edge profiles. The values are only given at the pixel locations.

are very similar, thus they can be represented by the same signature set. The signatures derived from the step edge response of the wavelet-based downsampling form the other signature set. These two sets are used for all images to try to identify the downsampling technique.

For each image to be upsampled, the algorithm computes the correlation coefficient between 4 × 4 blocks of the image and the blocks of each signature set. The correlation coefficient between blocks B_1 and B_2 is

$$C(B_1, B_2) = \frac{\mathrm{Cov}(B_1, B_2)}{\sigma_{B_1}\sigma_{B_2}},$$

where Cov(.) is the covariance and σ is the variance (the expectations are taken over the sample distribution of the blocks).

For each image block, the signature block with the highest correlation from each signature set gives the step edge response that "looks" most like the image block. This highest correlation is recorded for each image block and each signature set.

After the correlation values have been computed for all blocks in an image, the technique counts the number of blocks where the correlation coefficient is above a given threshold for each signature set. The downsampling technique whose signature set found more image blocks whose correlation coefficient is above the threshold will be declared as the subsampling method used for that image. Based on this assessment, the upsampling technique can be appropriately chosen.

4. Simulation results

Our proposed method was tested using 47 images. The images vary in size and content. They include natural indoors and outdoors images, close-up head images, synthetic images, satellite pictures, video scenes, and texture images.

In order to evaluate the accuracy of our technique, each image was downsampled by a factor of four using all three methods and the correlation-based matching technique was applied to each outcome. To speed up the computation, the correlation was only computed for blocks where the variance was above a given threshold indicating the possible presence of an edge. In these experiments a match is declared for a block (i.e. it is included in the count for the given signature set) if the correlation exceeds 0.992. This choice was motivated by our experiments and also ensures that only very strong matches are selected.

Table 2 in Appendix B lists for each image the counts of the number of 4 × 4 image blocks which had maximum correlation coefficient over 0.992 with signature blocks of the bilinear/DCT signature set (first number of each field) and the wavelet signature set (second number). For the bilinear and DCT cases a good identification is given if the first number is greater, i.e. more blocks of the image "looked like" step edge patterns of DCT/bilinear subsampling than those of wavelet-based subsampling. For the wavelet case it should be the reverse. In the case of a tie the decision is made for the wavelet method. The name of the images for which all three cases have been successfully identified is set in bold in Table 2.

As can be seen in that table, the number of matches at this level of fidelity varies greatly. For some images it is in the thousands (mostly synthetic images that contain more clear step edge patterns) while for others no match can be found at all.

The particular pattern choices yielded an overall accuracy of 66% for correctly identifying all three downsampling methods. The wavelet method was correctly found in 70% of all cases, the bilinear in 89%, and for the DCT case the method had an accuracy percentage of 91%.

5. Conclusion

In this paper we showed that the image quality after upsampling depends on both the downsampling method used to get the lower resolution image and the upsampling technique. We introduced a correlation-based technique for the identification of the subsampling method. Using an edge pattern, our method was able to accurately identify the downsampling method in 66% of the images used for all three downsampling techniques.

In future research more varied patterns can be used as well as investigating other differences in the edge regions of the downsampled images for improved accuracy.

Appendix A

Results of different upsampling and downsampling combinations are given in Table 1.

Table 1
PSNR (dB) comparison of different downsampling–upsampling combinations

Image	Method	Bilinear	DCT	Wavelet
Aerial	Bilinear	24.356	26.196	24.035
	DCT	23.999	26.809	23.887
	Wavelet	22.535	23.695	26.619
Aerial2	Bilinear	28.503	29.289	27.662
	DCT	28.123	29.794	27.635
	Wavelet	26.621	27.313	30.122
Apc	Bilinear	33.56	34.147	32.899
	DCT	33.189	34.617	32.826
	Wavelet	32.024	32.583	34.808
Aqua	Bilinear	25.489	25.931	24.596
	DCT	25.112	26.391	24.554
	Wavelet	23.817	24.295	26.557
Baboon	Bilinear	23.74	24.01	22.86
	DCT	23.33	24.49	22.84
	Wavelet	22.19	22.58	24.50
Balloon	Bilinear	29.431	30.975	28.839
	DCT	29.134	31.459	28.743
	Wavelet	27.416	28.435	31.983
Barbara	Bilinear	25.413	25.173	24.178
	DCT	24.955	25.657	24.272
	Wavelet	23.721	23.899	25.849
Beach	Bilinear	27.427	28.369	26.256
	DCT	27.073	28.86	26.194
	Wavelet	25.22	25.907	29.206
Bridge	Bilinear	25.67	26.48	24.84
	DCT	25.31	26.97	24.81
	Wavelet	23.85	24.56	27.19
Bwall	Bilinear	18.415	18.985	17.627
	DCT	18.057	19.456	17.641
	Wavelet	16.799	17.406	19.618
Camera	Bilinear	25.486	26.275	24.31
	DCT	25.141	26.763	24.287
	Wavelet	23.444	24.094	26.954
Coral	Bilinear	30.756	32.986	30.654
	DCT	30.434	33.593	30.528
	Wavelet	28.914	30.354	33.973
Crowd	Bilinear	29.643	32.668	28.751
	DCT	29.36	33.307	28.561
	Wavelet	27.017	28.41	34.019

Table 1 (*continued*)

Image	Method	Bilinear	DCT	Wavelet
Dna	Bilinear	33.683	33.685	30.312
	DCT	33.329	34.058	30.375
	Wavelet	30.655	30.889	33.282
Elaine	Bilinear	31.765	32.964	31.19
	DCT	31.47	33.387	31.131
	Wavelet	30.122	31.044	33.502
Fence	Bilinear	29.959	30.801	29.148
	DCT	29.611	31.264	29.084
	Wavelet	28.171	28.863	31.484
Finger	Bilinear	27.551	32.469	27.133
	DCT	27.281	33.435	26.841
	Wavelet	25.024	27.015	33.599
Front	Bilinear	26.52	28.415	25.989
	DCT	26.254	29.001	25.965
	Wavelet	24.376	25.567	29.615
Goldhill	Bilinear	30.37	31.351	29.414
	DCT	29.988	31.885	29.373
	Wavelet	28.384	29.172	32.096
Gray21	Bilinear	37.39	38.86	37.01
	DCT	37.53	39.08	37.19
	Wavelet	35.87	36.79	39.59
House2	Bilinear	23.951	24.935	23.244
	DCT	23.586	25.438	23.282
	Wavelet	22.148	23.054	25.675
Lake	Bilinear	27.66	29.73	27.36
	DCT	27.32	30.33	27.30
	Wavelet	25.72	27.10	30.75
Landsat	Bilinear	26.869	27.129	26.085
	DCT	26.501	27.558	26.087
	Wavelet	25.478	25.898	27.635
Lax	Bilinear	24.98	25.23	24.09
	DCT	24.60	25.68	24.08
	Wavelet	23.44	23.83	25.84
Lena	Bilinear	31.54	34.08	30.51
	DCT	31.24	34.70	30.31
	Wavelet	28.97	30.19	35.25
Linespr	Bilinear	32.709	35.143	32.53
	DCT	32.401	35.753	32.403
	Wavelet	30.692	32.159	36.316
Man	Bilinear	29.57	31.02	28.71
	DCT	29.23	31.54	28.60
	Wavelet	27.45	28.38	31.89
Meter	Bilinear	36.23	39.81	35.94
	DCT	35.96	40.57	35.71
	Wavelet	33.87	35.58	41.06
Moon	Bilinear	30.897	31.49	30.539
	DCT	30.533	31.95	30.51
	Wavelet	29.529	30.159	32.265
Pentagon	Bilinear	30.01	31.797	29.035
	DCT	29.682	32.344	28.889
	Wavelet	27.644	28.652	32.871
Peppers	Bilinear	31.242	33.213	31.008
	DCT	30.895	33.827	31.013
	Wavelet	29.425	30.847	34.139
Plane	Bilinear	29.67	32.21	29.33
	DCT	29.31	32.94	29.08
	Wavelet	27.71	29.05	32.16
Plants	Bilinear	29.85	30.61	27.94
	DCT	29.46	30.97	27.88
	Wavelet	27.33	27.82	31.15
Res_Chart	Bilinear	19.56	21.11	18.78
	DCT	19.34	21.37	18.74
	Wavelet	17.54	18.58	21.60
Ruler	Bilinear	12.866	14.78	14.093
	DCT	12.669	15.087	14.167
	Wavelet	12.608	14.922	14.308
Splash	Bilinear	33.18	35.72	33.37
	DCT	32.80	36.50	33.50
	Wavelet	31.47	33.38	36.41
Sthelens	Bilinear	25.501	27.156	24.672
	DCT	25.165	27.702	24.547
	Wavelet	23.312	24.33	28.127
Straw	Bilinear	17.151	18.554	15.198
	DCT	16.831	19.081	15.058
	Wavelet	14.193	14.884	19.528
Swimmer	Bilinear	34.852	35.274	33.406
	DCT	34.535	35.461	33.478
	Wavelet	32.683	33.233	35.963
Tajmahal	Bilinear	24.793	24.922	23.924
	DCT	24.411	25.353	23.96
	Wavelet	23.369	23.733	25.541

Table 1 (*continued*)

Image	Method	Bilinear	DCT	Wavelet
Tank	Bilinear	32.124	32.814	31.171
	DCT	31.757	33.29	31.122
	Wavelet	30.279	30.892	33.5
Test8g	Bilinear	15.984	15.921	15.172
	DCT	15.655	16.246	15.183
	Wavelet	14.869	15.037	16.218
Test8r	Bilinear	15.935	15.901	15.182
	DCT	15.614	16.216	15.186
	Wavelet	14.837	15.019	16.213
Tiffany	Bilinear	31.678	33.258	31.128
	DCT	31.296	33.933	30.89
	Wavelet	30.14	31.002	32.328
Warplane	Bilinear	34.335	35.926	33.069
	DCT	34.015	36.438	32.9
	Wavelet	31.889	32.759	36.814
Wgrain	Bilinear	18.029	18.82	16.952
	DCT	17.637	19.358	16.919
	Wavelet	15.977	16.641	19.6
Woman	Bilinear	37.368	41.262	37.217
	DCT	37.11	41.976	37.029
	Wavelet	35.065	36.93	42.465

The rows represent the downsampling method, and the columns the upsampling technique.

Appendix B

Simulation results are given in Table 2.

Table 2
Match count comparison for the test images

	DCT	Wavelet	Bilinear
Aerial	7/2	6/7	9/6
Aerial2	148/71	93/116	134/89
Apc	28/11	23/29	43/14
Aqua	8/0	2/18	20/0
Baboon	0/4	4/5	4/5
Balloon	150/10	14/153	162/13
Barbara	221/153	232/135	206/166
Beach	45/31	18/32	53/34
Bridge	171/105	147/161	187/115
Bwall	390/207	281/427	459/287
Camera	18/20	9/19	24/16
Coral	3/2	2/4	3/2
Crowd	38/14	45/16	48/17
Dna	1169/493	518/1228	1215/501
Elaine	37/20	28/70	94/18
Fence	257/228	191/246	237/169
Finger	55/0	13/42	61/2
Front	272/157	242/324	291/173
Goldhill	102/71	119/77	108/81
Gray21	1695/162	0/2636	1963/0
House2	139/83	110/137	138/45
Lake	116/107	137/121	121/125
Landsat	6/5	2/6	8/1
Lax	15/12	16/17	18/6
Lena	99/13	72/15	86/28
Linespr	113/87	115/146	140/97
Man	28/22	29/37	41/26
Meter	504/237	329/297	430/325
Moon	0/0	0/0	0/0
Pentagon	6/3	3/3	8/2
Peppers	67/41	47/51	76/44
Plane	97/43	81/105	105/47
Plants	469/163	167/390	462/115
Res_chart	321/278	379/404	399/265
Ruler	0/1	0/0	8/0
Splash	325/251	394/218	314/268
Sthelens	7/2	4/7	6/1
Straw	1/0	0/0	1/1
Swimmer	36/8	30/4	39/7
Tajmahal	19/8	2/9	34/1
Tank	9/17	27/3	13/5
Test8g	12/8	6/35	48/1
Test8r	12/0	3/24	31/1
Tiffany	4/2	4/6	6/4
Warplane	5/3	3/7	8/4
Wgrain	82/81	65/45	79/67
Woman2	22/2	12/11	13/13

The columns represent the downsampling method. The first number in each column is the count of image blocks with correlation over the given threshold with signature blocks for the bilinear/DCT signature set. The second number is the count for the wavelet signature set. Correct identification is made for DCT and bilinear cases if the first number is larger, and vice versa for the wavelet case.

References

[1] J.P. Allebach, P.W. Wong, Edge-directed interpolation, in: IEEE International Conference on Image Processing, Vol. 3, 1996, pp. 707–710.

[2] M. Antonini, M. Barlaud, P. Mathieu, I. Daubechies, Image coding using wavelet transform, IEEE Trans. Image Process. 1 (2) (1992) 205–220.

[3] C.B. Atkins, C.A. Bouman, J.P. Allebach, Tree-based resolution synthesis, in: Conference on Image Processing, Image Quality, Image Capture Systems, 1999, pp. 405–410.

[4] C.B. Atkins, C.A. Bouman, J.P. Allebach, Optimal image scaling using pixel classification, in: IEEE International Conference on Image Processing, Vol. 3, 2001, pp. 864–867.

[5] S.G. Chang, Z. Cvetković, M. Vetterli, Resolution enhancement of images using wavelet transform extrema extrapolation, in: International Conference on Acoustics, Speech and Signal Processing, 1995, pp. 2379–2383.

[6] R. Dugad, N. Ahuja, A fast scheme for image size change in the compressed domain, IEEE Trans. Circuits Systems Video Technol. 11 (4) (2001) 461–474.

[7] H.S. Hou, H.C. Andrews, Cubic splines for image interpolation and digital filtering, IEEE Trans. Acoust. Speech Signal Process. 26 (6) (1978) 508–517.

[8] K. Jensen, D. Anastassiou, Subpixel edge localization and the interpolation of still images, IEEE Trans. Image Process. 4 (3) (1995) 285–295.

[9] S.-H. Jung, S.K. Mitra, D. Mukherjee, Subband DCT: definition, analysis, and applications, IEEE Trans. Circuits Systems Video Technol. 6 (3) (1996) 273–286.

[10] R.G. Keys, Cubic convolution interpolation for digital image processing, IEEE Trans. Acoust. Speech Signal Process. 29 (6) (1981) 1153–1160.

[11] J. Mukherjee, S.K. Mitra, Image resizing in the compressed domain using subband DCT, IEEE Trans. Circuits Systems Video Technol. 12 (7) (2002) 620–627.

[12] J.A. Parker, R.V. Kenyon, D.E. Troxel, Comparison of interpolating methods for image resampling, IEEE Trans. Med. Imaging 2 (1) (1983) 31–39.

[13] M. Unser, A. Aldroubi, M. Eden, Enlargement or reduction of digital images with minimum loss of information, IEEE Trans. Image Process. 4 (3) (1995) 247–258.

[14] S. Yang, T.Q. Nguyen, Interpolated Mth band filters for image size conversion, in: IEEE International Conference on Image Processing, Vol. 3, 2001, pp. 891–894.